materials

MDPI

Communication

Production of Mn-Ga Magnets

Tetsuji Saito [1,*], Masahiro Tanaka [1] and Daisuke Nishio-Hamane [2]

[1] Graduate School of Engineering, Chiba Institute of Technology, Narashino 275-8588, Japan
[2] Institute for Solid State Physics, The University of Tokyo, Kashiwa 277-8581, Japan; hamane@issp.u-tokyo.ac.jp
* Correspondence: tetsuji.saito@it-chiba.ac.jp

Abstract: Mn-based magnets are known to be a candidate for use as rare-earth-free magnets. In this study, Mn-Ga bulk magnets were successfully produced by hot pressing using the spark plasma sintering method on Mn-Ga powder prepared from rapidly solidified Mn-Ga melt-spun ribbons. When consolidated at 773 K and 873 K, the Mn-Ga bulk magnets had fine grains and exhibited high coercivity values. The origin of the high coercivity of the Mn-Ga bulk magnets was the existence of the $D0_{22}$ phase. The Mn-Ga bulk magnet consolidated at 873 K exhibited the highest coercivity of 6.40 kOe.

Keywords: Mn-Ga alloys; melt spinning; spark plasma sintering; coercivity

Citation: Saito, T.; Tanaka, M.; Nishio-Hamane, D. Production of Mn-Ga Magnets. *Materials* **2024**, *17*, 882. https://doi.org/10.3390/ma17040882

Academic Editor: Joo Yull Rhee

Received: 21 December 2023
Revised: 7 February 2024
Accepted: 13 February 2024
Published: 14 February 2024

1. Introduction

Nowadays, high-performance rare-earth magnets (Nd-Fe-B magnets) are applied to various advanced devices, including hard disk drives, electric vehicles, and medical equipment [1–3]. Because regulations on internal combustion engines have been enacted or proposed in many countries, the production of electric vehicles with high-performance rare-earth magnet motors has significantly increased [4]. Under such circumstances, the continuously growing demand for rare-earth elements, which constitute an integral part of high-performance rare-earth magnets, has raised severe concerns due to their prices and availability, together with the hazardous nature of the mining and smelting of such elements [5–10]. These concerns have led to the study of new magnetic materials composed of rare-earth-free elements.

The performance of rare-earth-free magnets is expected to be worse than that of rare-earth magnets, but the less-hazardous nature of rare-earth-free magnets could make them good substitutes for rare-earth magnets in some applications not demanding a good performance [11]. The prospective candidates for rare-earth-free magnets with high earth abundance are iron-based and manganese-based magnets. There have been many efforts to develop new iron-based magnets, and the $L1_0$-FeNi intermetallic compound and α''-$Fe_{16}N_2$ nitrides have been identified as candidates for such magnets [12,13]. The current problem with the new iron-based magnets is the difficulty of their synthesis [14,15]. Until a new technique for their easy production is developed, these iron-based magnets are not considered highly promising.

On the other hand, manganese-based magnets have already been produced as commercial magnets [16]. More recently, manganese-based magnets, such as Mn-Ga magnets with a $D0_{22}$ phase and Mn-Bi magnets with a low-temperature phase (LTP), have been the focus of attention as prospective replacements for rare-earth magnets [17–26]. It has been reported that the Mn-Ga alloys produced by melt spinning consist of a $D0_{22}$ phase and exhibited high coercivity [27–33]. The advantage of Mn-Ga alloys is their high magneto-crystalline energy. Among the permanent magnets without rare-earth elements, Mn-Ga alloys possess the highest magneto-crystalline energy value, 2.6 MJ/m^3. Thus, Mn-Ga alloys are expected to show high coercivity.

In this study, we seek the possibility of producing Mn-Ga bulk magnets. Nd-Fe-B melt-spun ribbons are known to be consolidated into bulk Nd-Fe-B magnets by hot pressing [34–36]. Mn-Ga magnets can be expected to be obtained from melt-spun ribbons similarly. The structures and magnetic properties of the Mn-Ga magnets produced by hot pressing using the spark plasma sintering (SPS) method from melt-spun ribbons are described here.

2. Materials and Methods

Rapidly quenched melt-spun ribbons of $Mn_{65}Ga_{35}$ alloy were prepared in a quartz crucible using single-roller melt spinning apparatus (NEV-A01, Nissin Giken, Saitama, Japan). Rapid quenching was carried out with argon gas using a copper wheel (v_s = 50 ms^{-1}). Mn-Ga magnets were prepared from the rapidly quenched melt-spun ribbons. First, the rapidly quenched samples were mechanically comminuted into powders in an argon-filled glove box. The powders were then filled into carbon dies and consolidated in a vacuum at temperatures between 673 K and 973 K for 300 s using spark plasma sintering apparatus (Plasman, S. S. Alloy). A pressure of 100 MPa was applied during sintering.

The specimens were cooled to room temperature without applied pressure in the SPS chamber, and then pulled out from the carbon dies. After the surfaces of the specimens were cleaned using sandpaper, the properties of the specimens were examined. The density of the specimens was measured with Archimedes' method using an electronic balance (GR-120, AND). The phases of the specimens were determined by X-ray diffraction (XRD) with Cu K_α radiation using an X-ray diffractometer (MiniFlex600, Rigaku, Tokyo, Japan). The microstructures of the specimens were examined using a transmission electron microscope (TEM) (JEM-2100, JEOL, Tokyo, Japan) after ion beam thinning using an Ion Slicer (EM-09100IS, JEOL). The hysteresis loops of the specimens were examined using a vibrating sample magnetometer (VSM) (BHV-525RSCM, Riken Denshi, Tokyo, Japan).

3. Results and Discussion

Mn-Ga bulk magnets were successfully obtained from rapidly quenched Mn-Ga melt-spun ribbons by the SPS method. Figure 1 shows the dependence of the density and relative density of the Mn-Ga magnets on the consolidation temperature. The specimens had a density of about 6.4 g/cm^3 when consolidated at 673 and 723 K. In contrast, the specimens had a high density of 7.1–7.2 g/cm^3 when consolidated at 773 K or higher. These values represent approximately 97% of the ingot density. Since the typical density of Nd-Fe-B magnets produced by spark plasma sintering is 90–96% [29,30], the specimens consolidated at 773 K or higher had a sufficiently high density as magnets.

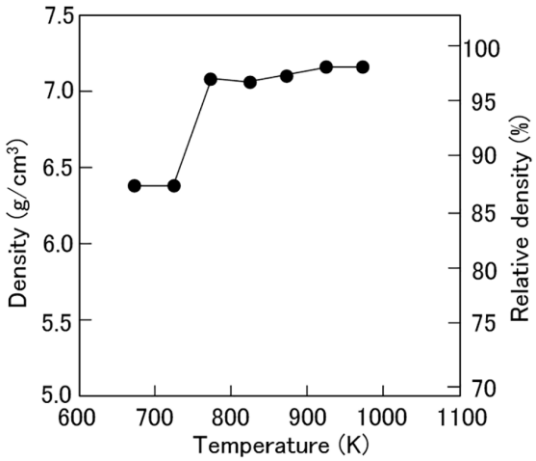

Figure 1. Dependence of the density and relative density of the Mn-Ga magnets magnet on the consolidation temperature.

Thus, the magnetic properties of the Mn-Ga magnets produced by consolidation at 773 K or higher were investigated. The consolidation temperature is a critical factor for not only the density of the magnets, but also the magnetic phase in the resultant Mn-Ga magnets. The dependence of the coercivity of the Mn-Ga magnets on the consolidation temperature is shown in Figure 2. The specimens showed high coercivity when consolidated at temperatures between 773 K and 873 K. In contrast, the specimens did not show high coercivity when consolidated at 923 K and higher. The Mn-Ga magnets consolidated at 873 K exhibited the maximum coercivity of 6.40 kOe in this experiment.

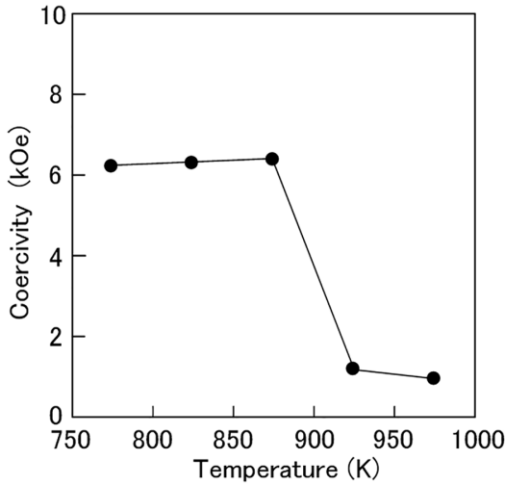

Figure 2. Dependence of the coercivity of the Mn-Ga magnets on the consolidation temperature.

Among the Mn-Ga alloys, intermetallic compounds, such as the hexagonal $D0_{19}$ phase, tetragonal $L1_0$ phase, and tetragonal $D0_{22}$ phase, have been investigated as magnetic materials [37]. Recently, it was found that the cubic $P4_132$ phase and cubic $P4_232$ phase exhibited high coercivity [38,39]. Figure 3 shows the XRD patterns of the Mn-Ga powder and the Mn-Ga magnets consolidated at 773 K, 873 K, and 973 K. The Mn_8Ga_5 and $D0_{19}$ phases' diffraction peaks were found in the Mn-Ga powder's XRD pattern, suggesting that the Mn-Ga powder consisted of the Mn_8Ga_5 and $D0_{19}$ phases. However, the $D0_{22}$ and $D0_{19}$ phases' diffraction peaks were seen in the Mn-Ga magnets' XRD patterns regardless of the consolidation temperature. This suggests that the Mn-Ga magnets consisted of the $D0_{22}$ and $D0_{19}$ phases. Although the Mn-Ga powder with the Mn_8Ga_5 and $D0_{19}$ phases did not show high coercivity, the Mn-Ga magnets with the $D0_{22}$ and $D0_{19}$ phases exhibited high coercivity. Thus, the origin of high coercivity in the Mn-Ga magnets is considered to be the $D0_{22}$ phase. The $D0_{22}$ phase in the Mn-Ga magnets was formed due to heat exposure, while consolidating the Mn-Ga powder. Although the Mn-Ga magnets were mainly composed of the $D0_{22}$ phase, they still contained some of the $D0_{19}$ phase. Since the prolonged annealing of Mn-Ga melt-spun ribbons—for seven days, for example—could increase the amount of the $D0_{22}$ phase [27], further optimization of the consolidation process can be expected to increase the amount of $D0_{22}$ phase in the Mn-Ga magnets.

Figure 4 shows TEM images of the Mn-Ga magnets consolidated at 773 K, 873 K, and 973 K. The specimens consolidated at 773 K had fine grains of around 0.5–1 μm in diameter, and the specimen consolidated at 873 K still consisted of fine grains of around 1–2 μm in diameter. On the other hand, the specimen consolidated at 973 K consisted of relatively large grains of around 5 μm in diameter. This indicates that grain growth was limited in the Mn-Ga magnet consolidated at 873 K, but significant grain growth occurred in the Mn-Ga magnet consolidated at 973 K. The Mn-Ga magnet consolidated between 773 K and 873 K consisted of fine grains of the $D0_{22}$ phase, and thus, exhibited high coercivities. This confirms that the optimal consolidation temperature to produce high-coercivity Mn-Ga magnets is between 773 K and 873 K.

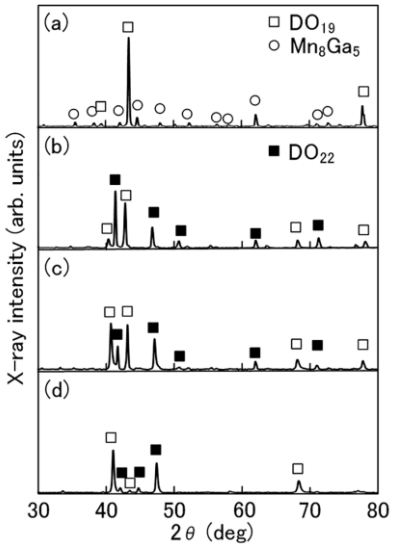

Figure 3. XRD patterns of (**a**) the Mn-Ga powder prepared from the Mn-Ga melt-spun ribbons and the Mn-Ga magnets consolidated at (**b**) 773 K, (**c**) 873 K, and (**d**) 973 K.

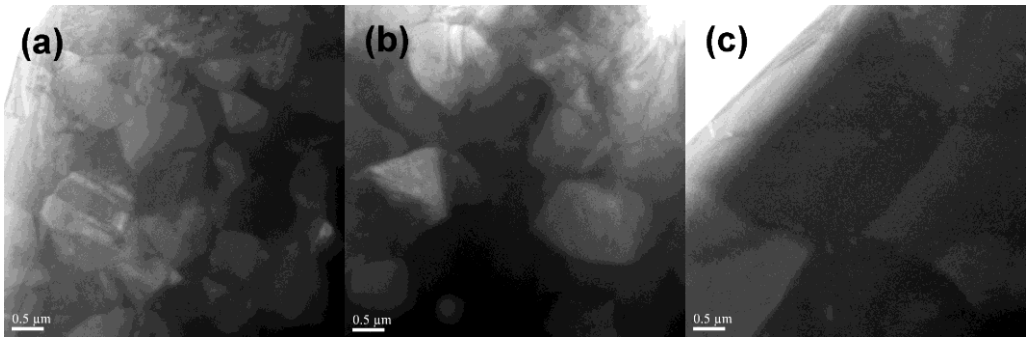

Figure 4. TEM images of the Mn-Ga magnets consolidated at (**a**) 773 K, (**b**) 873 K, and (**c**) 973 K.

Figure 5 shows the hysteresis loops of the Mn-Ga magnets consolidated at 773 K, 873 K, and 973 K, together with those of the Mn-Ga powder prepared from the rapidly quenched Mn-Ga melt-spun ribbons. The Mn-Ga powder did not show clear hysteresis, but the Mn-Ga magnets produced from the Mn-Ga powder exhibited hysteresis loops. The Mn-Ga magnet consolidated at 773 K showed a large hysteresis loop, with a coercivity of 6.20 kOe and a remanence of 17.9 emu/g, and the Mn-Ga magnet consolidated at 873 K also exhibited a large hysteresis loop, with a coercivity of 6.40 kOe and a remanence of 14.6 emu/g. The coercivity of 6.40 kOe achieved by the Mn-Ga magnet consolidated at 873 K was slightly smaller than that of the annealed Mn-Ga melt-spun ribbons (8 kOe) [27]. The Mn-Ga magnet consolidated at 973 K showed a relatively small hysteresis loop, with a coercivity of 1.05 kOe and a remanence of 2.55 emu/g. This suggests that the optimal consolidation temperatures to produce high-coercivity Mn-Ga magnets were between 773 K and 873 K.

There are several reports on the magnetic properties of Mn-Ga magnets. In the hot-compacted Mn-Ga magnets, a coercivity of 2.7 kOe was reported by T. Mix et al. [40]. In the cold-rolled Mn-Ga alloys, a high coercivity of 12.4 kOe was reported by S. Ener et al. [41] The high coercivity of the cold-rolled Mn-Ga alloy was achieved after magnetic annealing. The highest coercivity of 18.1 kOe was reported by J. Z. Wei et al. [42]. The Mn-Ga magnets with the highest coercivity have been produced by the long-term annealing of the Mn-Ga green compact, consolidated under a high pressure of 1.14 GPa. Therefore, magnetic or prolonged annealing can further improve the coercivity of the Mn-Ga magnets produced by the spark plasma sintering method.

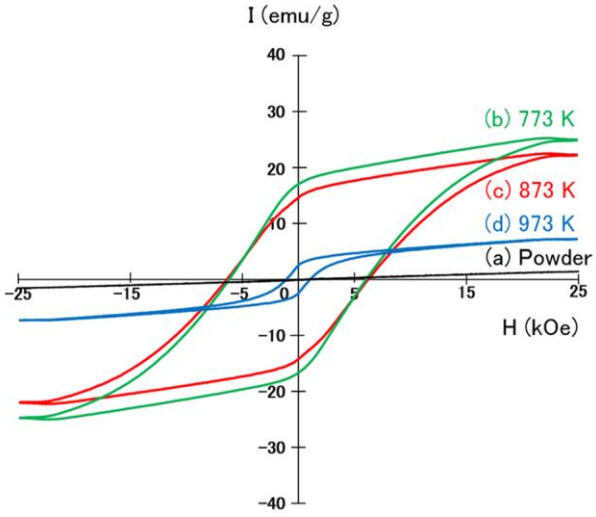

Figure 5. Hysteresis loops of (**a**) the Mn-Ga powder prepared from the Mn-Ga melt-spun ribbons and the Mn-Ga magnets consolidated at temperatures of (**b**) 773 K, (**c**) 873 K, and (**d**) 973 K.

4. Conclusions

Mn-Ga powder was prepared from rapidly quenched Mn-Ga melt-spun ribbons and consolidated into bulk magnets by the SPS method. It was found that the Mn-Ga bulk magnets had high densities of 7.1–7.2 g/cm^3 when consolidated at 773 K or higher. Although the Mn-Ga powder did not show clear hysteresis, the Mn-Ga magnets exhibited hysteresis loops. It was found that the Mn-Ga magnets comprised the $D0_{22}$ and $D0_{19}$ phases. The Mn-Ga bulk magnets consolidated at 773 K and 873 K had fine grains and exhibited high coercivity values, whereas those consolidated at 973 K had coarse grains and did not show high coercivity. The Mn-Ga bulk magnet consolidated at 873 K exhibited a maximum coercivity value of 6.40 kOe. However, the remanence of the Mn-Ga bulk magnets is not yet comparable to that of the typical permanent magnets. Further studies are therefore necessary to increase the remanence value.

Author Contributions: T.S.: methodology; formal analysis; original draft preparation. M.T.: methodology; investigation; formal analysis. D.N.-H.: investigation; formal analysis. All authors have read and agreed to the published version of the manuscript.

Funding: This research received no external funding.

Informed Consent Statement: Not applicable.

Data Availability Statement: Data are contained within the article.

Acknowledgments: The use of the facilities of the Materials Design and Characterization Laboratory at the Institute for Solid State Physics, The University of Tokyo, is gratefully acknowledged.

Conflicts of Interest: The authors declare no conflict of interest.

References

1. Bailey, G.; Mancheri, N.; Van Acker, K. Sustainability of Permanent Rare Earth Magnet Motors in (H)EV Industry. *J. Sustain. Met.* **2017**, *3*, 611–626. [CrossRef]
2. Sreenivasulu, K.V.; Srikanth, V.V.S.S. Fascinating Magnetic Energy Storage Nanomaterials: A Brief Review. *Recent Pat. Nanotechnol.* **2017**, *11*, 116–122. [CrossRef]
3. Yue, M.; Zhang, X.Y.; Liu, J.P. Fabrication of bulk nanostructured permanent magnets with high energy density: Challenges and approaches. *Nanoscale* **2017**, *9*, 3674–3697. [CrossRef] [PubMed]
4. Dong, S.Z.; Li, W.; Chen, H.S.; Han, R. The status of Chinese permanent magnet industry and R&D activities. *AIP Adv.* **2017**, *7*, 056237. [CrossRef]
5. Dutta, T.; Kim, K.-H.; Uchimiya, M.; Kwon, E.E.; Jeon, B.-H.; Deep, A.; Yun, S.-T. Global demand for rare earth resources and strategies for green mining. *Environ. Res.* **2016**, *150*, 182–190. [CrossRef]

6. Zhou, B.; Li, Z.; Chen, C. Global Potential of Rare Earth Resources and Rare Earth Demand from Clean Technologies. *Minerals* **2017**, *7*, 203. [CrossRef]
7. Alonso, E.; Sherman, A.M.; Wallington, T.J.; Everson, M.P.; Field, F.R.; Roth, R.; Kirchain, R.E. Evaluating Rare Earth Element Availability: A Case with Revolutionary Demand from Clean Technologies. *Environ. Sci. Technol.* **2012**, *46*, 3406–3414. [CrossRef] [PubMed]
8. Kötschau, A.; Büchel, G.; Einax, J.W.; von Tümpling, W.; Merten, D. Sunflower (*Helianthus annuus*): Phytoextraction capacity fir heavy metals on a mining-influenced area in Thuringia, Germany. *Environ. Earth Sci.* **2014**, *72*, 2023–2031. [CrossRef]
9. Miller, J.R. Forensic assessment of metal contaminated rivers in the 21st century using geochemical and isotopic traces. *Minerals* **2013**, *3*, 192–246. [CrossRef]
10. Okabe, T.H. Bottlenecks in rare metal supply and the importance of recycling—A Japanese perspective. *Miner. Process. Extr. Met.* **2017**, *126*, 22–32. [CrossRef]
11. Coey, J.M.D. Permanent magnets: Plugging the gap. *Scr. Mater.* **2012**, *67*, 524–529. [CrossRef]
12. Néel, L.; Pauleve, J.; Pauthenet, R.; Laugier, J.; Dautreppe, D. Magnetic Properties of an Iron—Nickel Single Crystal Ordered by Neutron Bombardment. *J. Appl. Phys.* **1964**, *35*, 873–876. [CrossRef]
13. Kim, T.K.; Takahashi, M. New Magnetic material having ultrahigh magnetic moment. *Appl. Phys. Lett.* **1972**, *20*, 492–494. [CrossRef]
14. Mizuguchi, M.; Kojima, T.; Kotsugi, M.; Koganezawa, T.; Osaka, K.; Takanashi, K. Artificial Fabrication and Order Parameter Estimation of L10-ordered FeNi Thin Film Grown on a AuNi Buffer Layer. *J. Magn. Soc. Jpn.* **2011**, *35*, 370–373. [CrossRef]
15. Ogawa, T.; Ogata, Y.; Gallage, R.; Kobayashi, N.; Hayashi, N.; Kusano, Y.; Yamamoto, S.; Kohara, K.; Doi, M.; Takano, M.; et al. Challenge to the Synthesis of α''-$Fe_{16}N_2$Compound Nanoparticle with High Saturation Magnetization for Rare Earth Free New Permanent Magnetic Material. *Appl. Phys. Express* **2013**, *6*, 073007. [CrossRef]
16. Ohtani, T.; Kato, N.; Kojima, S.; Kojima, K.; Sakamoto, Y.; Konno, I.; Tsukahara, M.; Kubo, T. Magnetic properties of Mn–Al–C permanent magnet alloys. *IEEE Trans. Magn.* **1977**, *13*, 1328–1330. [CrossRef]
17. Saito, T. Magnetic properties of Mn–Al–C alloy powders produced by mechanical alloying. *J. Appl. Phys.* **2005**, *97*, 10F304. [CrossRef]
18. Wei, J.Z.; Song, Z.G.; Yang, Y.B.; Liu, S.Q.; Du, H.L.; Han, J.Z.; Zhou, D.; Wang, C.S.; Yang, Y.C.; Franz, A.; et al. τ-MnAl with high coercivity and saturation magnetization. *AIP Adv.* **2014**, *4*, 127113. [CrossRef]
19. Rial, J.; Villanueva, M.; Cespedes, E.; Lopez, N.; Camarero, J.; Marshall, L.G.; Lewis, L.H.; Bollero, A. Application of a novel flash-milling procedure for coercivity development in nanocrystalline MnAl permanent magnet powders. *J. Phys. D Appl. Phys.* **2017**, *50*, 105004. [CrossRef]
20. Saito, T.; Nishimura, R.; Nishio-Hamane, D. Magnetic properties of Mn–Bi melt-spun ribbons. *J. Magn. Magn. Mater.* **2014**, *349*, 9–14. [CrossRef]
21. Ly, V.; Wu, X.; Smillie, L.; Shoji, T.; Kato, A.; Manabe, A.; Suzuki, K. Low-temperature phase MnBi compound: A potential candidate for rare-earth free permanent magnets. *J. Alloys Compd.* **2014**, *615*, S285–S290. [CrossRef]
22. Anand, K.; Pulikkotil, J.J.; Auluck, S. Effects of inter-site chemical disorder on the magnetic properties of MnBi. *J. Magn. Magn. Mater.* **2014**, *363*, 18–20. [CrossRef]
23. Poudyal, N.; Liu, X.; Wang, W.; Nguyen, V.V.; Ma, Y.; Gandha, K.; Elkins, K.; Liu, J.P.; Sun, K.; Kramer, M.J.; et al. Processing of MnBi bulk magnets with enhanced energy product. *AIP Adv.* **2016**, *6*, 056004. [CrossRef]
24. Sakuma, A. Electronic structures and magnetism of CuAu-type MnNi and MnGa. *J. Magn. Magn. Mater.* **1998**, *187*, 105–112. [CrossRef]
25. Saito, T.; Nishimura, R. Hard magnetic properties of Mn–Ga melt-spun ribbons. *J. Appl. Phys.* **2012**, *112*, 083901. [CrossRef]
26. Lu, Q.M.; Yue, M.; Zhang, H.G.; Wang, M.L.; Yu, F.; Huang, Q.Z.; Ryan, D.H.; Altounian, Z. Intrinsic magnetic properties of single-phase $Mn_{1+x}Ga$ ($0 < \times < 1$) alloys. *Sci. Rep.* **2015**, *5*, 17086.
27. El-Gendy, A.A.; Hadjipanayis, G. High Coercivity in Annealed Melt-Spun Mn–Ga Ribbons. *IEEE Trans. Magn.* **2014**, *50*, 1. [CrossRef]
28. Yang, J.; Yang, W.; Shao, Z.; Liang, D.; Zhao, H.; Xia, Y.; Yang, Y. Mn-based permanent magnets. *Chin. Phys. B* **2018**, *27*, 117503. [CrossRef]
29. Lu, Q.M.; Wang, D.J.; Li, C.H.; Zhang, H.G.; Yue, M. Recrystallization induced coercivity and magnetic properties enhancement in hot-deformed L1-$Mn_{1.8}Ga$ magnet. *J. Magn. Magn. Mater.* **2019**, *474*, 167–172. [CrossRef]
30. Hao, L.; Xiong, W. An evaluation of the Mn–Ga system: Phase diagram, crystal structure, magnetism, and thermodynamic properties. *Calphad* **2020**, *68*, 101722. [CrossRef]
31. Keller, T.; Baker, I. Manganese-based permanent magnet materials. *Prog. Mater. Sci.* **2022**, *124*, 100872. [CrossRef]
32. Thanh, P.T.; Ngoc, N.H.; Lam, N.M.; Hau, K.X.; Yen, N.H.; Anh, T.V.; Dan, N.H. Structure and magnetic properties of melt-spun Mn–Ga–Cu–Al ribbons. *Mater. Res. Express* **2023**, *10*, 086101. [CrossRef]
33. Kirste, G.; Freudenberger, J.; Wurmehl, S. Phase transformation in Mn_3Ga considering different degrees of deformation. *Acta Mater.* **2023**, *258*, 119025. [CrossRef]
34. Lee, R.W.; Brewer, E.G.; Schaffel, N.A. Processing of Neodymium-Iron-Boron melt-spun ribbons to fully dense magnets. *IEEE Trans. Magn.* **1985**, *21*, 1958–1963. [CrossRef]

35. Saito, T.; Takeuchi, T.; Kageyama, H. Structures and magnetic properties of Nd–Fe–B bulk nanocomposite magnets produced by the spark plasma sintering method. *J. Mater. Res.* **2004**, *19*, 2730–2737. [CrossRef]
36. Mo, W.; Zhang, L.; Shan, A.; Cao, L.; Wu, J.; Komuro, M. Microstructure and magnetic properties of NdFeB magnet prepared by spark plasma sintering. *Intermetallics* **2007**, *15*, 1483–1488. [CrossRef]
37. Huh, Y.; Kharel, P.; Shah, V.R.; Krage, E.; Skomski, R.; Shield, J.E.; Sellmyer, D.J. Magnetic and Structural Properties of Rapidly Quenched Tetragonal $Mn_{3-x}Ga$ Nanostructures. *IEEE Trans. Magn.* **2013**, *49*, 3277–3280. [CrossRef]
38. Brown, D.R.; Han, K.; Siegrist, T. Hard magnetic properties observed in bulk $Mn_{1-x}Ga_x$. *J. Appl. Phys.* **2014**, *115*, 17A723. [CrossRef]
39. Saito, T.; Nishio-Hamane, D. New hard magnetic phase in Mn–Ga–Al alloy. *J. Alloys Compd.* **2015**, *632*, 486–489. [CrossRef]
40. Mix, T.; Müller, K.-H.; Schultz, L.; Woodcock, T.G. Formation and magnetic properties of the L10 phase in bulk, powder and hot compacted Mn–Ga alloys. *J. Magn. Magn. Mater.* **2015**, *391*, 89–95. [CrossRef]
41. Ener, S.; Skokov, K.P.; Karpenkov, D.Y.; Kuz'Min, M.D.; Gutfleisch, O. Magnet properties of $Mn_{70}Ga_{30}$ prepared by cold rolling and magnetic field annealing. *J. Magn. Magn. Mater.* **2015**, *382*, 265–270. [CrossRef]
42. Wei, J.Z.; Wu, R.; Yang, Y.B.; Chen, X.G.; Xia, Y.H.; Yang, Y.C.; Wang, C.S.; Yang, J.B. Structural properties and large coercivity of bulk $Mn_{3-x}Ga$ ($0 \leq \times \leq 1.15$). *J. Appl. Phys.* **2014**, *115*, 15–18. [CrossRef]